AGU PUBLICATIONS

JGR

Journal of Geophysical Research: Space Physics

TECHNICAL REPORTS: METHODS

10.1002/2016JA022487

Special Section:
Measurement Techniques in Solar and Space Physics: Photons

Key Points:
- A new class of spaceborne imaging spectrometers has been developed, an integral field spectrograph (IFS)
- An IFS can simultaneously obtain three dimensions of measurements of two spatial and one spectral dimensions
- An IFS can be specially suited to study explosive, unpredictable events in Heliophysics, Earth Science, and Astrophysics

Correspondence to:
P. C. Chamberlin,
Phillip.C.Chamberlin@NASA.gov

Citation:
Chamberlin, P. C., and Q. Gong (2016), An integral field spectrograph utilizing mirrorlet arrays, *J. Geophys. Res. Space Physics*, *121*, 8250–8259, doi:10.1002/2016JA022487.

Received 3 FEB 2016
Accepted 14 SEP 2016
Accepted article online 16 SEP 2016
Published online 28 SEP 2016

An integral field spectrograph utilizing mirrorlet arrays

Phillip C. Chamberlin[1] and Qian Gong[2]

[1]Heliophysics Division, Solar Physics Laboratory, NASA Goddard Space Flight Center, Greenbelt, Maryland, USA, [2]Instrument Systems and Technology Division, NASA Goddard Space Flight Center, Greenbelt, Maryland, USA

Abstract An integral field spectrograph (IFS) has been developed that utilizes a new and novel optical design to observe two spatial dimensions simultaneously with one spectral dimension. This design employs an optical 2-D array of reflecting and focusing mirrorlets. This mirrorlet array is placed at the imaging plane of the front-end telescope to generate a 2-D array of tiny spots replacing what would be the slit in a traditional slit spectrometer design. After the mirrorlet in the optical path, a grating on a concave mirror surface will image the spot array and provide high-resolution spectrum for each spatial element at the same time; therefore, the IFS simultaneously obtains the 3-D data cube of two spatial and one spectral dimensions. The new mirrorlet technology is currently in-house and undergoing laboratory testing at NASA Goddard Space Flight Center. Section 1 describes traditional classes of instruments that are used in Heliophysics missions and a quick introduction to the new IFS design. Section 2 discusses the details of the most generic mirrorlet IFS, while section 3 presents test results of a lab-based instrument. An example application to a Heliophysics mission to study solar eruptive events in extreme ultraviolet wavelengths is presented in section 4 that has high spatial resolution (0.5 arc sec pixels) in the two spatial dimensions and high spectral resolution (66 mÅ) across a 15 Å spectral window. Section 4 also concludes with some other optical variations that could be employed on the more basic IFS for further capabilities of this type of instrument.

1. Introduction

A primary science objective for many missions in the NASA Heliophysics System Observatory (HSO) aims to study fast, solar eruptive events (SEEs). These very rapid energy releases occur over large spatial areas and with different spectral responses for different emissions. Current instruments, due to the reality of two-dimensional detectors, are limited to two dimensions of information. If spectral information simultaneously with two spatial dimensions could be achieved, then images and videos could be used to study topology and dynamics of the SEEs as well as the spectral information of various lines to determine line-of-sight motions (Doppler), heating (line broadening), density changes (line ratios), etc. Most instruments that look at the photon output of the Sun can generally be categorized into four existing types, which are described below, followed by a new, fifth type that is the topic of this paper. These five classes are summarized in Table 1.

A spectrometer is the simplest class that only obtains a single wavelength on a single-element detector and provides no spatial information or "Sun as a star" measurements. These use a band-pass filter to restrict the wavelength range of the spectrum that is measured by the detector, usually a photodiode. Some examples of these instruments are the EUV spectrophotometer (ESP) [*Didkovsky et al.*, 2012] on the Solar Dynamics Observatory (SDO) [*Pesnell et al.*, 2012] Extreme Ultraviolet Variability Experiment (EVE) [*Woods et al.*, 2012], the X-Ray Photometer System (XPS) [*Woods et al.*, 2008] on the Thermosphere Ionosphere Mesosphere Energetics and Dynamics (TIMED) solar EUV experiment (SEE) [*Woods et al.*, 2005], and the X-Ray Sensors (XRS) [*Garcia*, 1994; *Chamberlin et al.*, 2009] on the GOES spacecraft. An alternate design utilizes a rotating grating or translating single-element detector to measure a single wavelength at any time but is capable of building a spectrum using multiple measurements over a given time. One example of this is the Solar Radiation Climate Experiment (SORCE) Solar Stellar Irradiance Comparison Experiment (SOLSTICE) [*McClintock et al.*, 2005].

A spectrograph is a second class that simultaneously measures one full dimension of spectral information on either a 1-D or 2-D detector but is also incapable of providing spatial information. Some examples of these

Table 1. A Summary of the Solar Photon Instrumentation Types[a]

	Number of Dimensions		
	Spatial	Spectral	Total
Spectrometer	0	0	0
Spectrograph	0	1	1
Imager	2	0	2
Spectral imager	1	1	2
Integral field spectrograph	2	1	3

[a]These range from single-element instruments, spectrometers, and gradually increase the number of spectral and spatial dimensions up to the three-dimensional instruments that are the focus of this paper, the integral field spectrograph.

instruments are SDO EVE Multiple EUV Grating Spectrographs (MEGS) [*Woods et al.*, 2012] and the TIMED SEE EUV Grating Spectrograph (EGS) [*Woods et al.*, 2005]. Spectrographs utilizing 2-D detectors often use the second dimension in the cross-dispersion direction to increase the signal by placing a slit as the entrance aperture and an imaging grating that images this slit to provide more light onto the detector while using the width of the slit to control spectral resolution. While these instruments often can measure a very large set of free-free emission lines and free-bound and bound-bound continua that are valuable for studying solar eruptive events [*Chamberlin et al.*, 2012; *Ryan et al.*, 2013; *Milligan et al.*, 2014], they are limited from having no spatial information to know where the plasma that is emitting is located.

The third class of instruments is the imager that includes a telescope with a 2-D detector. Two example imagers are those on the SDO Atmospheric Imaging Assembly (AIA) [*Lemen et al.*, 2012] and Helioseismic and Magnetic Imager (HMI) [*Schou et al.*, 2012] and another example imager being the Transition Region and Coronal Explorer (TRACE) [*Handy et al.*, 1999]. These imagers measure two spatial dimensions, where a band-pass filter or interferometer is often used to isolate a single, specific emission line or larger range of wavelengths. A filter wheel can be used in the same channel to look at other emissions or bands, but the information will not be synchronous in time. Alternatively, multiple instruments or channels can be used to provide synchronous images at multiple wavelengths, such as with SDO AIA, but the resources required become increasingly heavy, costly, and complex so the opportunities to fly this type of mission are rare.

A fourth class is a spectral imager, which is a hybrid of the two aforementioned classes, can measure one spatial dimension and the other spectral. Examples of these instruments are Solar and Heliospheric Observatory (SOHO) Solar Ultraviolet Measurements of Emitted Radiation (SUMER) [*Wilhelm et al.*, 1997], Hinode EUV Imaging Spectrograph (EIS) [*Culhane et al.*, 2007], and the Interface Region Imaging Spectrograph (IRIS) [*De Pontieu et al.*, 2014]. This complex combination has a front-end imaging telescope that provides an image onto a narrow slit, where the narrow image that makes it through the slit defines the spatial information. The back end of these instruments disperse the slit image off a grating, where the slit is perpendicular to the grating dispersion direction, and reimage back onto a detector to provide a spectrum for each spatial element along slit. These instruments can either "sit-and-stare mode" when science focus is on spectral dynamics or in "scan mode" where a second spatial dimension is desired. These spatial scans often confuse spatial information with temporal changes as the complete 2-D image is not at the same time.

The fifth class of instruments, which is the focus of this paper, is referred to as integral field spectrographs (IFSs) and is a combination of the other three classes. This new IFS design starts with a front-end imaging telescope that provides an image at a plane. But at this image plane, where a slit would have been placed in a slit spectrometer, the IFS has a two-dimensional array of hundreds to thousands of small mirrors, or "mirrorlets," each element being its own imaging telescope and defining the 2-D spatial elements of the IFS. Each of these mirrorlet spatial elements is diffracted off of a focusing grating that is reimaged onto a detector. This mirrorlet is the single most important optical change that leads to two spatial dimensions, defined by the mirrorlet, and one spectral dimension for each spatial point, all simultaneously obtained on a single 2-D detector. The IFS has the potential, limited only by the signal, to obtain high spectral and 2-D spatial resolution. It is also a fully reflective optical system, meaning it can extend down to EUV and up to infrared wavelengths that are excluded with refractive optics. This instrument also has the advantage of no moving parts, such as scan mirrors, and does not require constant observatory scanning so would be cheaper to implement and be more reliable.

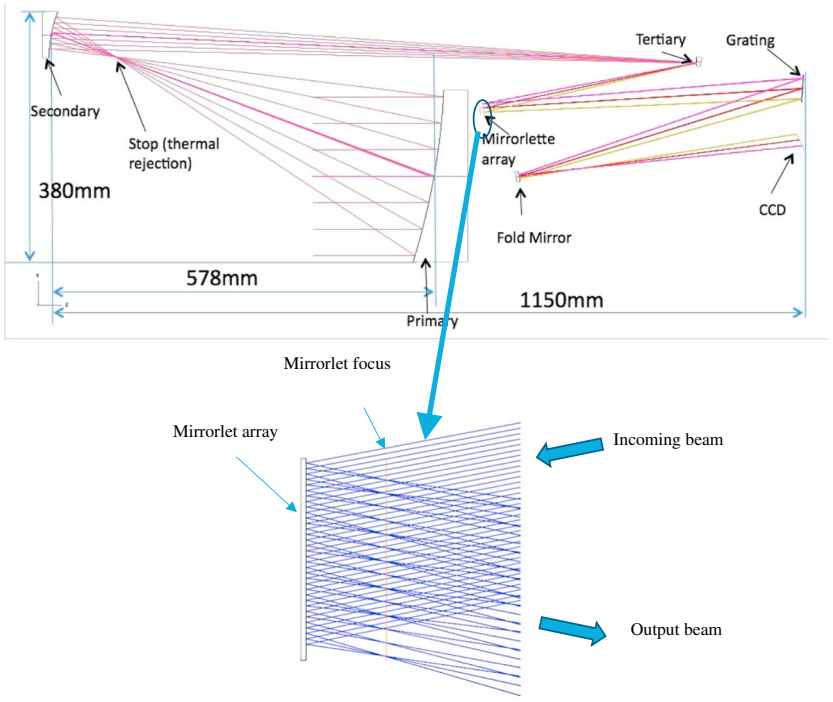

Figure 1. Optical layout of IFS. The incident beam with an extralarge *f*/# is imaged on the mirrorlet array surface. Due to such a large *f*/#, the PSF covers a number of mirrorlets. For each individual mirrorlet, the incident light is equivalent to a collimated beam. The mirrorlet focal plane is shown in the blownup picture of the mirrorlet array.

2. Mirrorlet Integral Field Spectrograph

2.1. Three-Dimensional Integral Field Spectrograph

Currently, there are three main types of IFSs that have different ways of isolating the spatial locations prior to feeding the spectrograph optics. The three primary ways to isolate the spatial locations are using a lenslet array [*Bacon et al*., 1995; *Larkin et al*., 2006], image slicers [*Weitzel et al*., 1996], and a lenslet array that feeds fibers [*Roth et al*., 2005]. However, none of these three types works for EUV application. The lenslet array and the combination of lenslet array and fibers do not pass EUV wavelengths. The image slicer, in principle, can be designed as an all-reflective system. But in reality, the relatively low reflectivity of each prevented the complicated multimirror system being used for EUV application; therefore, the mirrorlet array was invented to replace the lenslet array to achieve the high throughput EUV or Infrared [*Gong et al*., 2015] IFS.

The IFS consists of a front-end telescope and a back end spectrometer, where an example optical design produced in Zemax can be seen in Figure 1. Some components in Figure 1 are not necessary, such as the fold and Tertiary mirrors, but this design gives a good general concept of the necessary components of an all-reflective IFS—a primary mirror, a mirrorlet array, a imaging grating, and a detector.

The first optical subsystem is a focusing telescope. This subsystem uses an off-axis Gregorian telescope to create an intermediate image at the focus of the primary mirror. This focal plane is used to insert a thermal stop to reduce the solar radiation beyond the field of view (FOV) on the much smaller secondary mirror. This telescope and its elements are also designed to provide the correct magnification so that the instrument image size can be defined as it falls on the next optical element, the mirrorlet. The number of smaller mirrorlet elements required within this array will be defined by the spatial and spectral resolution from the science requirements. From the spatial resolution point of view, one mirrorlet is equivalent to one pixel on detector arrays.

An example mirrorlet array has been procured to test, and some of the specific design features and test results will be discussed in section 3. The substrate of this mirrorlet array is fused silica to allow etching to occur at high accuracy. An array of small concave mirrors is plasma etched into the substrate and coated with high EUV reflectivity materials. The function of the mirrorlets is to focus the portion of the telescope image on

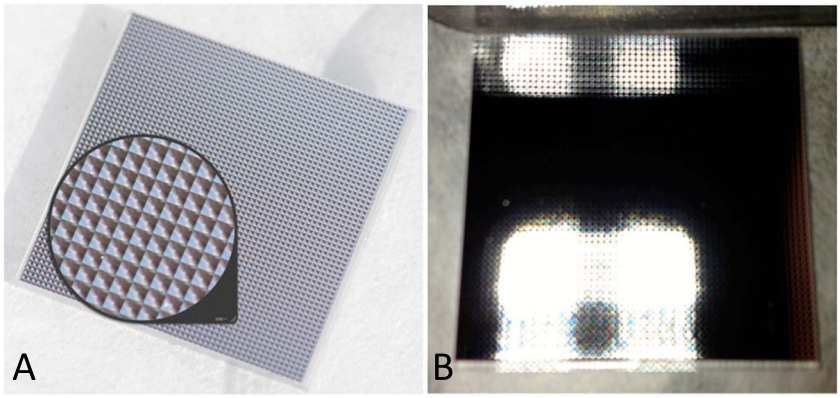

Figure 2. Pictures of an example mirrorlet array. (a) The 50 × 50 elements, with a magnifying glass over a portion to provide details. (b) This array after an Al vapor coating to increase its reflectivity.

each mirrorlet into a tiny spot, so enough space is made for laying the spectral traces. It should be mentioned that the object of the IFS is not the original image plane of the telescope; it is the dot array in the focal plane of mirrorlets. The mirrorlet array size is 0.267 × 0.267 mm and the focal length is 4.8 mm. An example mirrorlet array with 2500 (50 × 50) mirrolette elements can be seen in Figure 2. Figure 2a shows a picture of this array, which also include a magnifying glass to zoom in on a portion and provide more details. Figure 2b shows this array after an Al coating was applied in order to increase the reflectivity of these reflectors. A slit is used at the imaging plane of a slit spectrometer in order to define the FOV, but in the IFS this mirrorlet is used instead in the imaging plane to define not only the FOV of the instrument based on what part of the image falls on the overall mirrorlet but also each individual element also provides the spatial resolution elements/pixels. If there is a 50 × 50 element mirrorlet array, the final image is going to have 2500 spatial elements spread equally in the two spatial dimensions, assuming they are not limited by optical elements further down the line. The size of each mirrorlet is determined by the length of each spectrum, detector pixels size, and the number of rows to avoid crosstalk. So the telescope plate scale is designed to ensure that the specified FOV matches the mirrorlet array size, and the *f*/# of the telescope guarantees the sampling for the spatial resolution.

The mirrorlet is at the imaging plane, so once the light is reflected off of these elements, it is first converged to an array of tiny dots (point spread function (PSF) of mirrorlet). This array of dots is the object of the spectrometer. This step makes an originally continuous image become an array of dots, therefore providing the space for laying out the spectra. The light will start diverge after mirrorlet focus and continues to propagate onto the detector through the spectrometer optical path.

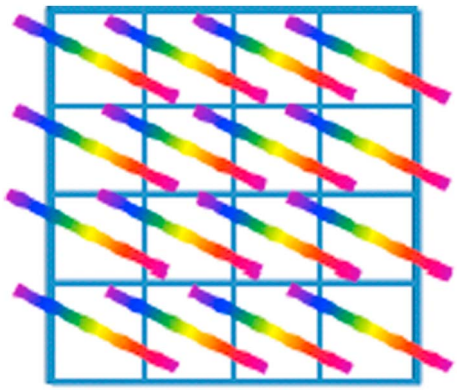

Figure 3. A cartoon example showing the final image on the detector from a 4 × 4 spatial array IFS. Each line represents the full spectrum for each spatial pixel. The mirrorlet is slightly tilted with respect to the detector to avoid spectra from adjacent pixels from overlapping.

The next optical element encountered in the IFS after the mirrorlet array is a grating. This grating disperses every spatial element so that each has its own spectrum. In this case, the grating used also had power to it in order to reimage the light onto the detector. A planar grating could have been used, followed by another focusing mirror, but the imaging grating provides the ability to combine two optical elements into one while still meeting the instrument requirements. This is significant for the optical system at EUV for increasing the throughput.

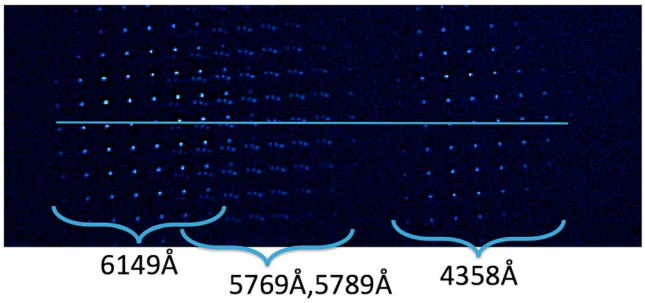

Figure 4. The 3-D data cube from an IFS using a Mercury lamp, where the horizontal blue line shows a single spectrum that is along the dispersion direction. The mirrorlet is slightly rotated with respect to the dispersion direction so that spectra from two corresponding spatial mirrorlets do not overlap, which is why the image of each set of spectral emissions looks slightly tilted with respect to this artificial blue line. This figure is therefore similar to Figure 3 being rotated, so each spectrum in Figure 3 is horizontal.

The dispersed light is next focused on the detector. A cartoon example can be seen in Figure 3. Each line, or spectrum, is from a single spatial pixel and mirrorlet. The spectrum from each spatial element is spread out across the detector as seen by the lines. In order for the spectra for adjacent spatial pixels to not overlap, the mirrorlet is rotated at a slight angle, as can be seen in Figure 3. The power of each mirrorlet ensures that there is spatial separation between each of the spectra so they do not overlap. The band pass of the spectrum, defined by coatings, band-pass filters, and the grating density, is optimized in an IFS such that each spectrum does not fully cross the detector as well, and only is significant in a portion to also ensure spectra for various spatial pixels do not overlap.

3. Lab Testing of an IFS

3.1. Mirrorlet Development

The mirrorlet itself has been a large development effort at NASA/GSFC over the past 2 years as it has application not only to Heliophysics but also in Earth Science, Astrophysics, and Planetary studies. There have been no problems encountered in the microlithography and etching technique as evident through discussion, obtaining, and testing. An Aluminum reflective coating was also applied via vapor deposition in order to increase is reflectivity. As of July 2013 a patent application for mirrorlets has been submitted. This internal effort has significantly help improve the optical quality of the optical surfaces, where the surface roughness for the 4 μm depth of each of the Lyman Alpha Solar Spicule Observatory (LASSO) mirrorlets has been measured to be less than 1.25 nm. This optical quality will have no adverse effects on the image quality given this surface roughness and the spatial/spectral resolution of the instrument.

The current technology provides the means for fabricating the mirrorlet that meets the IFS requirements. As we know that the RMS wavefront error of any optical surface is a function of its size. Depending upon the type of aberration, it can be second, third, or fourth order of the radius. For mirrorlet, the size is so tiny, so the surface figure never becomes an issue. PSFs created by all mirrorlets are diffraction limited. As for the radius of curvature, it is not a critical parameter for this application. The error due to reactive ion etching usually is proportional to its designed depth. That means, the figure of the surface is still spherical, and it is the same for all mirrorlets. The importance for this application is that the curvatures for all mirrorlets are the same within the depth of focus of the mirrorlet to make sure the PSFs from all mirrorlets are in the same plane.

3.2. Lab Optical Test Results

To verify the mirrorlet concept and avoid using vacuum chamber, the optical test is performed in visible. Figure 4 shows an example image from the IFS setup in the lab. This spectral image uses a Mercury discharge lamp, which is collimated, focused, and reflected off the mirrorlet. The entire 50×50 element array was originally illuminated, but to simplify presentation for viewing here a circular aperture was placed to limit the field of view to approximately 81 spatial elements spanning the two dimensions or approximately a 9×9 grid. These mirrorlet images are sent to a grating before being imaged onto the charged-couple device (CCD) or other detector. This limited image FOV was performed solely to simplify the analysis when initially identifying what spectral emission goes with what 2-D imaging elements.

The spatial circular "image" group on the right is the strong Hg emission line at 4358 Å, while the bright image group on the left is the strong 6149 Å line. In between these two distinct spectral images are the doublet 2-D images at 5769 Å and 5789 Å as well as another, dimmer emission line at 5460 Å (not labeled). As described in section 2, the mirrorlet is slightly tilted with respect to the dispersion direction, so that the

Table 2. Optical Parameters for the LASSO Telescope

Parameters	Values
EFL at mirrorlet array	59 m
f/# at mirrorlet array	227
f/# at CCD	45
FOV	1.0 × 0.75 arc min
Wavelength range	1205.0 Å–1220.0 Å
Emissions of interest (peak formation Temp. in log(T))	121.57 nm—H Lyman-alpha (4.5) 120.65 nm—Si III (4.9) 121.83 nm—O V (5.3)
Spatial resolution	0.5″ × 0.5″ pixels
Spectral resolution	33 mÅ/pixel
Grating period	2400 cycles/mm (blazed to second order)
Grating radius of curvature	800 mm
Mirrorlet array	60 × 45 with 267 μm square pixels
CCD	2048 × 2048 with 13.5 μm pixels

dispersed spectral lines from adjacent FOV points do not overlap with other emission lines from other spatial points. The horizontal line seen in Figure 4 traces the spectrum for a single spatial point (near the middle of the nine-element diameter image) across the spectrum.

3.3. Calibration and Data Reduction

Existing techniques would be utilized and adapted for determining both the radiometric calibration of the instrument as well as a spectral/wavelength map of each detector pixel. One example is the data reduction software developed for Goddard lenslet IFS project, the Goddard Imager and Integral Field Spectrometer (GIFS) on Apache Point Observatory as well as used for another breadboard of a visible mirrorlet IFS.

4. LASSO Example IFS

4.1. Science Questions

Science questions that an IFS is particularly well suited to address have to do with very rapid, explosive events where spatial variations are different and the occurrence of such events are unpredictable. Solar flares observations with an orbital instrument are ideal, as these explosions occur on time scales that are faster than a scanning spectrometer can provide repeat scans. Also, the chance that the slit is located or scanning correctly to catch the initial events as the onset of the flare also limits the events observed. The imaging provided by the IFS would also allow spectral comparisons of the different spatial locations of foot points, loops, loop-tops, and above the loop-top regions that evolve quickly near a flare event. The IFS would also provide spectral images along the loop arcade as well as along foot point ribbons that have their own timing sequences that may be lost if having to scan or only have a spectrometer with no imaging capabilities.

4.2. LASSO Design

Solar flares are a natural phenomenon that can take advantage of an IFS, but there is a need to increase the technology readiness level (TRL) and prove the IFS design prior to the more expensive and rare orbital instrument has a chance of selection. One way to do this TRL increase of the IFS is on a sounding rocket, but the chances of catching a flare on a 5 min observation that the timing of this launch is planned months in advance is extremely rare; therefore, a science focus could be on spicule formation, transport, and heating through the solar chromosphere to coronal. Spicules are also short-lived explosive events but are always present on the Sun.

A sounding rocket payload was developed and proposed to measure spicule and was called the Lyman Alpha Solar Spicule Observatory (LASSO). This more specifically looked at the on-disk counterparts of spicules, referred to as rapid blueshifted events [*Rouppe van der Voort et al*., 2009] as they were formed in the transition region at temperatures in the few tens of thousands of Kelvin, then are heated to single MegaKelvin as they move up into the solar atmosphere [*De Pontieu et al*., 2011] and could potentially deposit heat and mass into the Corona as a source of coronal heating. A description of the optical design and observations can be seen in Table 2.

LASSO takes advantage of three strong emission lines, with formation temperatures ranging in the high chromosphere to the corona, all within a stated band pass. The imaging capabilities of the IFS allowed LASSO to track many individual spicules throughout their heating to get motions transverse to the plane. The three different spectral emissions allowed the heating to be observed as the spicule disappeared from one spectral

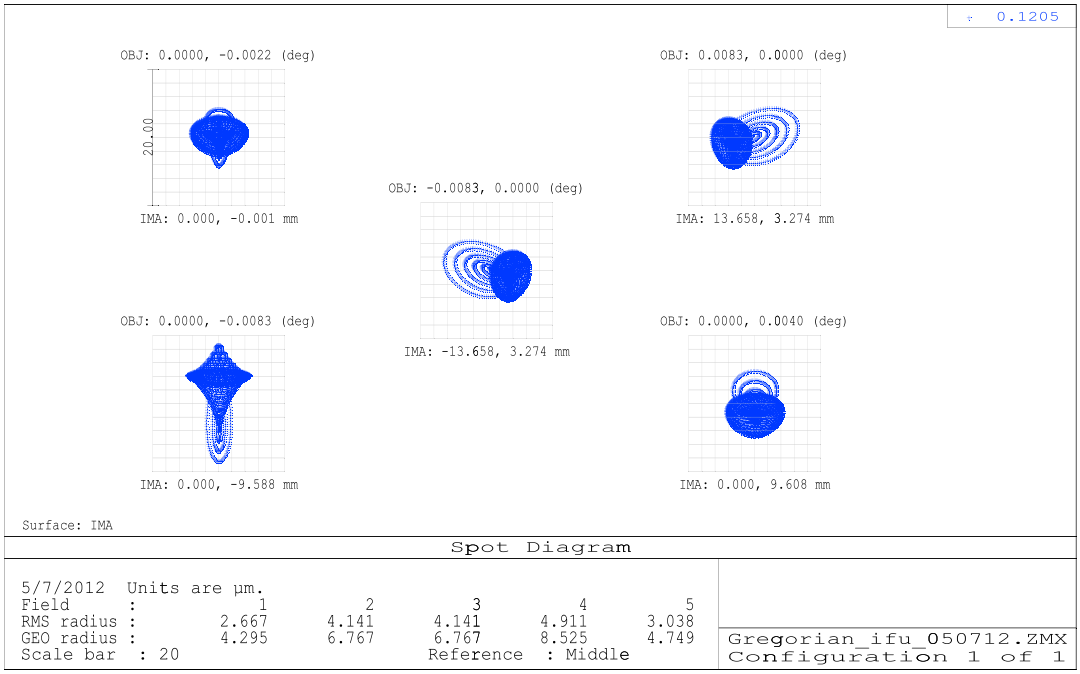

Figure 5. The spot diagram, from Zemax, demonstrating the optical spread of a given element from the IFS on the detector plane.

image into another image of higher temperature. The high spectral resolution will also allow for Doppler line of sight and rotational velocities to be computed when combined with the 2-D images.

The LASSO telescope is a Gregorian design with a primary, secondary, and tertiary mirrors that has a focal point beyond the primary as seen in Figure 2, and many of the LASSO optical specifications can be seen in Table 1. The main optical components in the Gregorian telescope are two off-axis parabolas and have heritage on large number of NASA missions so are at TRL 9.

At the focus of the telescope is a 60×45 two-dimensional array of tiny focusing mirrors that define the 2700 spatial elements of the imager, where each mirrorlet directs each spatial element onto the grating. This mirrorlet array is similar to the one shown in Figure 2. The light is spectrally dispersed while being simultaneously reimaged by a focusing grating on to a CCD detector. A fold mirror is in place between the imaging grating and the detector to achieve a much longer focal length in a smaller length rocket payload—leading to a smaller mass payload and higher altitude and longer observing while not affecting optical quality. The fold mirror also allows the warm end of the cooled CCD to be against the vacuum bulkhead to ease the cooled CCD thermal design. The focusing grating provides diffraction limited point spread function (PSF) and desired spectral dispersion to make sure the spectral resolution can be achieved. Figure 5 shows the spot diagram on the CCD. Figure 6 shows that the spectral dispersion for wavelength range 1205 Å to 1220 Å is close to 6.1 mm, which is equivalent to 455 pixels over 15 Å wavelength range. There is also a narrow spectral band-pass filter in order to limit light outside of the band pass. This filter is not able to be narrow enough to eliminate all the other wavelengths outside of the range that appear in Figure 7 without reducing the Lyman-alpha signal itself to the point where it is dominated by noise. This is a mature design that has been the focus of NASA/GSFC internal funding.

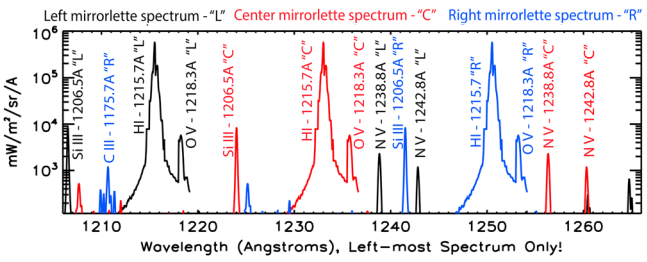

Figure 6. The solar spectrum as seen in one complete row (dispersion direction) of LASSO data. One row comprises three mirrorlets and, therefore, three overlapping spectra with different wavelength scales.

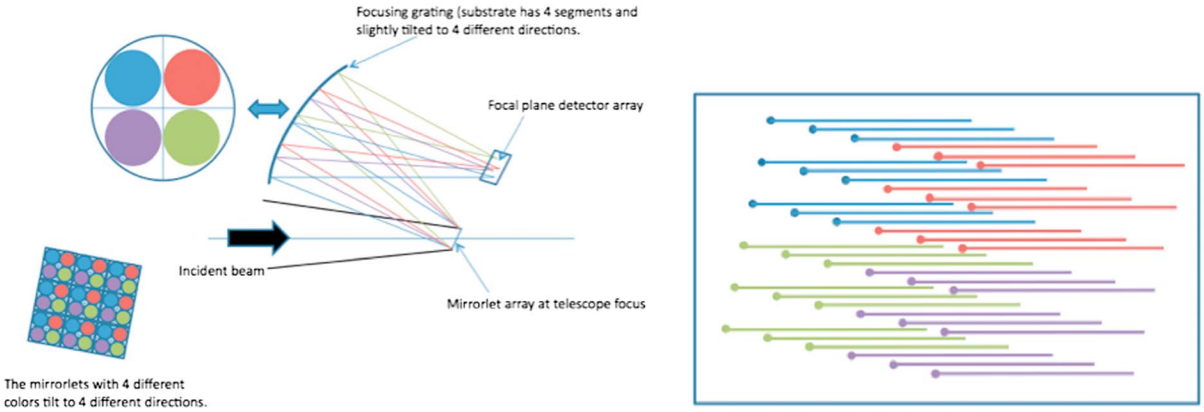

Figure 7. A version of the mirrorlet IFS that contains four separate optical paths. Each path is produced by each quadrant of a 2×2 set, which defines a spatial pixel, being etched at a different angle. As seen in the picture, each blue, red, purple, and green adjacent 2×2 elements define a "spatial element," while each color is at the same angle and power and will have its own defined spectral range and resolution. Each color goes on its own optical path but then is refocused on the detector as seen on the right side of the figure.

The LASSO mirrorlet array provides an imaging resolution of 45 spatial elements in the dispersion direction and 60 spatial elements in the cross-dispersion direction. Each LASSO mirrorlet will produce a 455-pixel spectrum that is less than a pixel tall (although will spread out over two pixels), with a single dark row in between to separate each spectra. The mirrorlet array is clocked in such a way that the spectrum from each subsequent spatial mirrorlet in the dispersion direction falls above the spectrum from each mirrorlet to the left and shifted by 0.5″ spatially. The spatial pixels size on the sky is determined by the size of the mirrorlets and the size of the image at the telescope focus, which for LASSO is equivalent of 0.5″ in each direction. The two-dimensional spatial image also has a filling factor of 100%, meaning there is no loss of spatial information due to the etching production of each individual mirrorlet element. The physical size of the mirrorlet is 267 μm and its focal length is designed at 7.6 mm, which provides a *f*/45 beam at the CCD to match the CCD's 13.5 μm pixel size.

The final image on the CCD is spectral dispersion of each spatial mirror from the mirrorlet; therefore, the image quality of the telescope is not critical as long as it is much smaller than the mirrorlet size of 267 μm square. The fabrication and alignment tolerance for the telescope primary, secondary, and tertiary mirrors can easily be met. The Zemax Monte Carlo analysis indicates that the tolerance on focusing grating is not very tight either due to the large *f*/# of *f*/45. All these reduce the cost and risk to the mission and guarantee focus to be held throughout the flight.

The image quality of the spectrometer is critical, because it determines the spectral resolution and crosstalk between adjacent spectra. Figure 5 shows the spot diagram of the spectrometer on the detector plane. The spot size meets the required specification of the RMS radius being smaller than the pixel size (or diameter being smaller than two pixels).

A simulated "row" of data from the LASSO IFS can be seen in Figure 6. This shows the spectra that lie along a given CCD row and are from three different mirrorlet elements, which corresponds to three different spatial pixels. Each pixel is color coordinated into red, blue, and black. The optical design and spectral dispersion were designed so that major spectral lines do not overlap. The bottom axis is the signal-to-noise cutoff, whereby below this axis the detector noise dominates. All three lines required for the science investigation, the O V, Si III, and H I, can be see for each of the three spatial elements, as well as other lines that may contribute extra science.

4.3. IFS Variations Examples

The IFS described previously is one of the simplest implementations and a baseline IFS design. It is very simple to increase the complexity for other IFS designs by taking advantage of the flexibility when etching the mirrorlets. One variation is to etch different angles or powers for each of the mirrorlets where each different angle/power is focused in a different direction. The design can coordinate different "sets," such as a 2×2 pattern of mirrorlets that can be seen in Figure 7. Each 2×2 set would define a single spatial element, but each

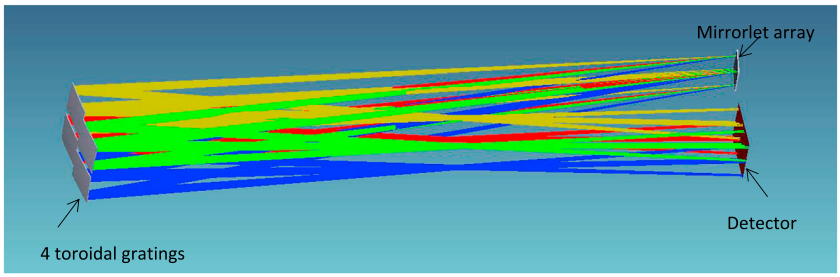

Figure 8. An example four channel mirrorlet IFS design. The mirrorlet array is at the telescope focus and focuses the light on each mirrorlet to a tiny point after mirrorlet array. Four adjacent mirrorlets were binned as a unit with each mirrorlet within tilted at a different angle. After the four beams are separated, four focusing gratings are added. The four focusing gratings are also tilted differently in order to position the four spectral images on one square detector.

quadrant (seen as color coordinated in the cartoon in Figure 7) would have a single angle or power different from the other quadrants. This setup will send the beam to different spectrometer paths, which may contain a different grating ruling or band pass, or contain different polarization filters. These then can be focused on their own, independent detectors, or coordinated in a way to fall back on the same, shared detector as shown in Figure 7 (right). The top left spectrum of each blue, green, red and purple seen in Figure 7 is its own optimized spectral range and resolution but is from the same spatial element in the image.

More specifically for this example, an image could be formed on a mirrorlet where the spatial resolution is defined by each 1×2 element pair, with every other element at a slightly different angle to form two separate paths for a given 1×2 spatial element. These two separate paths would then go to their own specialized grating and through a unique band-pass filter, then be reimaged back onto a single detector. One path may get a high-resolution spectral image of the He II 30.38 nm emission line that would also measure the Si XI 30.33 nm and Ca XVIII 30.22 nm emissions, while another path optimized for the strong H I 121.56 nm line would be observed that would also provide spectrally resolved measurements of the Si III 120.65 nm and 121.83 O V emission lines within the spectrum. This shows a way to get two-dimensional images of better than 1″ spatial resolution simultaneously of many emission lines throughout the chromosphere, transition region, and corona. The other distinct advantage of this technique is the high spectral resolution images that eliminate blends that are not available with traditional imagers.

Another quick example would be to expand the previous 1×2 element pairing into a 2×2 element pairing, reducing the number of spatial elements in half but adding two additional band passes and emission line sets. These two could even go off to a completely separate optical path with their own gratings at grazing incidence and their own detectors, opening up simultaneous spectral images at much shorter wavelengths in the EUV down into the EUV at around a few nm in wavelength. This would allow many more strong, hot flare lines that are present at these short wavelength to be observed, such as the ones that have recently been found by SDO/EVE [*Woods et al*., 2011], albeit this time with the additional spatially resolved information provided by the IFS.

It should be noted that all mirrorlets that tilt to the same direction must have the same power or focal length. This is to make sure that the object consisting of an array of tiny dots is in a same flat plane. Only in this condition, high spatial and spectral resolution can be achieved in the detector plane.

Another advantage of this setup is that it provides more space for spectral dispersion. In other words, it increases the spectral resolution without satisfying the spatial resolution. The trade-off is that multiple channels mean more optics. Even though the number of optical elements in each channel is not changed, so is the throughput, but the overall instrument becomes larger. But, given that the front-end telescope is the same, the design is still a large resource savings over multiple, completely independent telescopes. Figure 8 shows such a four channel IFS design.

5. Conclusions

An IFS can be a very powerful tool in order to view explosive events as it simultaneously provides two spatial dimensions and one spectral dimension. This optical design also provides this 3-D data cube without any

moving parts, simplifying instrument design and operations. A general description of the basic IFS was given, as well as specific example for a Lyman-alpha IFS with high spatial and spectral resolution, showing its usefulness in providing new Heliophysics observations. A brief discussion also demonstrated the flexibility of an IFS for more complex instruments due to the ease of etching the mirrorlet for different angles and powers. This technique is flexible and can be used in a wide range of application across Heliophysics, Earth Science, and Astrophysics.

Acknowledgments
This work was support under NASA Goddard Space Flight Center's Internal Research and Development (IRAD) program. The authors would like to thank RPC Photonics for producing the mirrorlet array. No data were used in producing this manuscript.

References

Bacon, R., et al. (1995), 3D spectrography at high spatial resolution. I. Concept and realization of the integral field spectrograph TIGER, *Astron. Astrophys. Suppl.*, *113*, 347.

Chamberlin, P. C., T. N. Woods, F. G. Eparvier, and A. R. Jones (2009), Next generation x-ray sensor (XRS) for the NOAA GOES-R satellite series, *Proc. SPIE*, *7438*, 743–802, doi:10.1117/12.826807.

Chamberlin, P. C., R. O. Milligan, and T. N. Woods (2012), Thermal evolution and radiative output of solar flares observed by the EUV variability experiment (EVE), *Sol. Phys.*, *279*(1), 23–42, doi:10.1007/s11207-012-9975-y.

Culhane, J. L., et al. (2007), The EUV imaging spectrometer for Hinode, *Sol. Phys.*, *243*(1), 19–61, doi:10.1007/s01007-007-0293-1.

De Pontieu, B., S. W. McIntosh, M. Carlsson, V. H. Hansteen, T. D. Tarbell, P. Boerner, J. Martinez-Sykora, C. J. Schrijver, and A. M. Title (2011), The origins of hot plasma in the solar corona, *Science*, *331*, 55, doi:10.1126/science.1197738.

De Pontieu, B., et al. (2014), The imaging region imaging spectrograph (IRIS), *Sol. Phys.*, *289*(7), 2733–2779, doi:10.1007/s11207-014-0485-y.

Didkovsky, L., D. Judge, S. Wieman, T. Woods, and A. Jones (2012), EUV spectrophotometer system (ESP) in extreme ultraviolet variability experiment (EVE): Algorithms and calibrations, *Sol. Phys.*, *275*(1–2), 179–205, doi:10.1007/s11207-009-9485-8.

Garcia, H. A. (1994), Temperature and emission measure from GOES soft X-ray measurements, *Sol. Phys.*, *154*(2), 275–308, doi:10.1007/BF00681100.

Gong, Q., et al. (2015), The prototype imaging spectrograph for coronagraphic exoplanet studies (PISCES) for WFIRST/AFTA, *Proc. SPIE 9605*, Techniques and Instrumentation for Detection of Exoplanets VII, 96050G (September 11, 2015).

Handy, B. N., et al. (1999), The Transition Region and Coronal Explorer (TRACE), *Sol. Phys.*, *187*(2), 229–260, doi:10.1023/A:1005166902804.

Larkin, J., et al. (2006), OSIRIS: A diffraction limited integral field spectrograph for Keck, *New Astron. Rev.*, *50*, 362–364, doi:10.1016/J.newar.2006.02.005.

Lemen, J. R., et al. (2012), The atmospheric imaging assembly (AIA) on the Solar Dynamics Observatory (SDO), *Sol. Phys.*, *275*(1), 17–40, doi:10.1007/s11207-011-9776-8.

McClintock, W. E., G. J. Rottman, and T. N. Woods (2005), Solar Stellar Irradiance Comparison Experiment II (SOLSTICE II): Instrument concept and design, *Sol. Phys.*, *230*(1), 225–258, doi:10.1007/s11207-005-1585-5.

Milligan, R. O., G. S. Kerr, B. R. Dennis, H. S. Hudson, L. Fletcher, J. C. Allred, P. C. Chamberlin, J. Ireland, M. Mathioudakis, and F. P. Keenan (2014), The radiated energy budget of chromospheric plasma in a major solar flare deduced from multi-wavelength observations, *Appl. J.*, *793*(2), 70, doi:10.1088/0004-637X/793/2/70.

Pesnell, W. D., B. J. Thompson, and P. C. Chamberlin (2012), The Solar Dynamics Observatory (SDO), *Sol. Phys.*, *275*(1), 3–15, doi:10.1007/s11207-011-98441-3.

Roth, M. M., et al. (2005), PMAS: The Potsdam multi-aperture spectrophotometer. I. Design, manufacture, and performance, *Publ. Astron. Soc. Pac.*, *117*, 620–642, doi:10.1086/429877.

Rouppe van der Voort, L., J. Leenaarts, B. de Pontieu, M. Carlsson, and G. Vissers (2009), On-disk counterparts of type-II spicules in the Ca II 854.2 nm and Hα lines, *Appl. J.*, *705*, 272, doi:10.1088/0004-637X/705/1/272.

Ryan, D. F., P. C. Chamberlin, R. O. Milligan, and P. T. Gallagher (2013), Decay-phase cooling and inferred heating of M- and X-class solar flares, *Appl. J.*, *778*(1), 68, doi:10.1088/0004-637X/778/1/68.

Schou, J., et al. (2012), Design and ground calibration of the Helioseismic and MagneticImager (HMI) instrument on the Solar Dynamics Observatory (SDO), *Sol. Phys.*, *275*(1), 229–259, doi:10.1007/s11207-011-9842-2.

Weitzel, L., A. Krabbe, H. Kroker, N. Thatte, L. E. Tacconi-Garman, M. Cameron, and R. Genzel (1996), 3D: The next generation near-infrared imaging spectrometer, *Astron. Astrophys. Suppl.*, *119*, 531–546, doi:10.1051/aas:1996266.

Wilhelm, K., et al. (1997), First results of the SUMER telescope and spectrometer on SOHO—I. Spectra and spectroradiometry, *Sol. Phys.*, *170*(1), 75–104, doi:10.1023/A:1004923511980.

Woods, T. N., F. G. Eparvier, S. M. Bailey, P. C. Chamberlin, J. Lean, G. J. Rottman, S. C. Solomon, W. K. Tobiska, and D. L. Woodraska (2005), Solar EUV experiment (SEE): Mission overview and first results, *J. Geophys. Res.*, *110*, A01312, doi:10.1029/2004JA010765.

Woods, T. N., et al. (2008), XUV Photometer System (XPS): Improved solar irradiance algorithm using CHIANTI spectral models, *Sol. Phys.*, *250*(2), 235–267, doi:10.1007/s11207-008-9196-6.

Woods, T. N., et al. (2011), New solar extreme-ultraviolet irradiance observations during flares, *Appl. J.*, *739*(2), 59, doi:10.1088/0004-637X/739/2/59.

Woods, T. N., et al. (2012), Extreme Ultraviolet Variability Experiment (EVE) on the Solar Dynamics Observatory (SDO): Overview of science objectives, instrument design, data products, and model developments, *Sol. Phys.*, *275*(1), 115–143, doi:10.1007/s11207-009-9487-6.